https://doi.org/10.53655/joe.c1987k

Jurnal OptoElektronik

Identification of C-H Bond Vibration Mode Using Absorption Spectroscopy By A Simple Optically Configured Setup

N. Ali Hasim[1,2,*], S. A. Aljunid[2], N. A. M. Ahmad Hambali[1,2], C. B. M. Rashidi[2] and R. Endut[2]

[1]*Semiconductor Photonics & Integrated Lightwave Systems, Faculty of Electronic Engineering Technology, Universiti Malaysia Perlis*
[2]*Centre of Excellence Advanced Communication Engineering - Optics Group, University Malaysia Perlis*
[*]*Corresponding author*: norshamsuri@unimap.edu.my

Keywords

Absorption spectrum
Interferometer
Spectrometer

Article History

Received: 4 June 2021
Accepted: 9 July 2021
Published: 15 July 2021

Abstract

An optical system model for the identification of Carbon-Hydrogen bond using spectroscopy is demonstrated and applied to the experiment setup. The optical simulation is achieved using simulation software and performed in a two-mirror system. The optical setup covers a wavelength range of 600 nm to 1200 nm which is a new study based on carbon-hydrogen bond and test with samples from several groups. Significant results of the Carbon-Hydrogen bond at 1149 nm are detected in Dichloromethane and ethanol. This observation is recorded in real-time and applied in a fast diagnostic system. The isosbestic point of water is measured at 970 nm and useful for our system spectral calibration. The result also shows the ability to quantify the chemical bond of a sample based on two peaks of absorption due to the C-H bonding. This gives a better opportunity for Chemometrics to perform accurately.

1. Introduction

Spectroscopy is the interaction of an electromagnetic wave with matter[1]. This study relates to the effect of absorption, emission, or scattering of electromagnetic radiation. The system was founded by Newton in 1655 [2] and then developed to be an analytical instrument by Bunsen and Kirchhoff in 1959 for flame spectroscope [3]. The spectroscopy was initially started with a study of flame samples. A similar technique was also used by other researchers who studied spectra of stars and sparks [2].

The spectroscopy is determined by the wavelength or the frequency of light. The basic principle can be anticipated from the experiment of the photoelectric effect [4] which shows that the response on a certain matter is not contributed by an intensity of the light but rather by its wavelength as based on the equation below:

$$E = \frac{hc}{\lambda}. \tag{1}$$

It is shown that there is a transfer of energy and it can be classified based on the response on the wavelength.

Spectroscopy has been widely used as an instrumental measurement to study chemical bonds. It is very useful in various fields such as photonics, agriculture, chemical, and medical discipline. In the medical field, spectroscopy provides spectra for solid and liquid samples with no pretreatment, able to implement continuous methodologies, swiftly provide spectra and predict physical and chemical parameters from a single spectrum. These attributes make it especially attractive for straightforward, speedy characterization of samples.

The wavelength of our system is near-infrared (NIR) which has reflection ranging from 650 nm until 1200 nm. NIR spectroscopy is challenging since most of the vibration modes that fall in this wavelength region are overtones modes either in second harmonic or third harmonics [5], [6]. The C-H vibration bond is normally detected using Mid Infrared (MIR) signal since the fundamental vibration modes of the C-H bond fall under this wavelength. MIR spectrometer is normally bulky and expensive on the tools and sources used. The sample preparation might be difficult since it not homogenous on the micron size sample [7]. However, the NIR spectrometer offers the simplicity of the experimental setup, the availability of the source which is cheaper, and easy preparation made the system is more demanding. This experimental setup can be seen in Section 2.2. The C-H bond is one of the important chemical bonds which relate to many medical or chemical studies. The C-H molecular vibration was used to analyze human

tumors such as glioblastoma, brain metastases of melanoma, and breast cancer which induced in an orthotropic mouse model[8].

Most of the studies on C-H bond vibration concentrated on the high wavenumber spectral region 2400 - 3800 cm^{-1} (2600 nm - 4200 nm)[8]–[10] that fall under MIR region. However, to our knowledge, no one studies the C-H bond vibration on our wavelength configuration due to the many harmonic overtones and a fall almost close to third harmonics. Besides, the NIR spectrometer provides an unusually fast response to this bond, usually taking less than 1 s, compared to analytical techniques. It also requires, no sample preparation and it is nondestructive. This result can be inspected in the spectrometer when the concentration of the analyte exceeds about 0.1%[11].

The spectral measurement in this dedicated wavelength is focused on identifying the C-H bond vibrational mode. The diagnosis from the spectral of C-H bond can benefit analyses of tissue malignancies for early cancer detection. This simple setup allows simple pre-measurement of tissue malignancies which then can be incorporated with chemometrics analysis for an accurate result. There are also studies [6], [12]–[15]related cancer detection using C-H bond which uses other methods and also Mid Infrared source which shown advantages of this bonding toward cancer research. This initial finding can bring forward and extend for early cancer detection.

2. Methods

This experimental study is divided into two stages. The initial stage is optical modeling using optical simulation software. Then, the second stage is the experimental realization. The experimental setup is implemented in few iterations together with the simulation. The configuration setup is the initial model in simulation software before implemented in the optical table. This propose setup is based on viability experimental work, then the optical setup has been optimized using simulation software to achieve higher efficiency and high optical power received at the optical detector. The simulation was used to test and optimize, the lens configuration and setup layout. In this simulation study, the two mirrors system was used to optimize the space requirement. It also gives better alignment by using more mirrors. The optical setup can be adjusted easily for a compact optical system if it using two mirrors instead of the one mirror technique. Once the simulation result was finalized, the optical components were installed on an optical table and the alignment optimization was done through the photodetector to get the highest coupling efficiency. During alignment of optical setup, some sampling was used as experiment reference to achieved higher visibility of optical output and optical absorption.

2.1 Simulation

Initially, our experimental setup was modeled using optical modeling and simulation (Zemax). The initial optical setup model was based on optical loss as shown in Fig 1. The power alignment and the focus point on each lens and mirror were simulated. The optical loss was calculated based on the received power spectrum at the photodetector. The loss of optical signal due to air, lenses, and mirrors was calculated and the signal received value must not be further from the calculation value. Optical loss due to misalignment in modeling was identified and reduced in this simulation. The optical loss was identified from the intensity of the light that goes through certain apparatus. This loss may due to the Gaussian beam divergence increase the area of space of interaction between material with the source. For example, the coating in the mirror will reduce the intensity and when the divergence occurs the mode field diameter will increase thus increasing the area of the interaction between the source and the lens.

$$\Delta\theta = \frac{w}{L_r}\left[1 + \left(\frac{L_r}{B}\right)^2 + \left(\frac{L_r A}{B}\right)^2\right]. \tag{2}$$

The above equation is the beam divergence which shown by $\Delta\theta$, where w is the beam waist, $L_r = \frac{\pi w^2}{\lambda}$ is the Rayleigh length, and A and B are the corresponding matrix elements. For propagation in free space $A = 1$ and $B = d$ so that $\Delta\theta \approx \lambda\sqrt{3}/\pi w$ for $d = L_r\Delta\theta \approx \lambda\sqrt{2}/\pi w(L_r/d)$ for $d \leq L_r$, and $\Delta\theta \approx \lambda/\pi w$ for $d \geq L_r$. The detail of beam divergence can be extract from [16], [17].

The placement of the correct lenses on the Equation (2) will improve the divergence and thus reduce the losses in the system. From this simulation, the position and placement of optical components were improved to get high coupling efficiency at the receiver side. The tungsten-halogen lamp was used as a light source to provide a broad dynamic range, however, it produced less power on each of the wavelengths of interest. Thus, to optimize the position and displacement of components, the alignment needs to be done carefully to achieve meaningful absorption spectra at the photodetector. In the simulation, the coupling efficiencies of the light going through lenses and mirrors into the photodetector were measured and optimized. The coating of lenses to allow only certain wavelengths into the lenses was studied. Such coating removes unintended wavelengths from pass through the lenses or optical mirror.

https://doi.org/10.53655/joe.c1987k

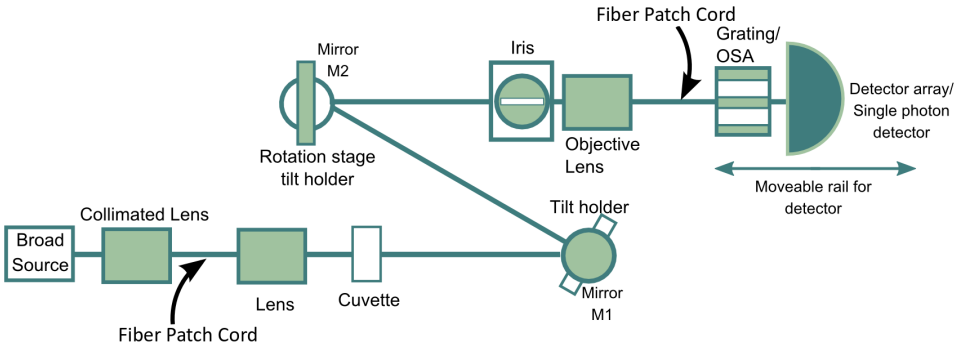

Figure 1. The optical setup test bed design for simulation and experimental setup.

Based on the simulation result, the coating on the mirror did not have a significant effect on the coupling efficiency at the receiver.

2.2 Experimental Setup

In the experiment, the optical setup was prepared to cover the NIR spectral region from 600 nm until 1200 nm. The wavelength selection was based on the optical components to cover visible and short NIR regions. A broad

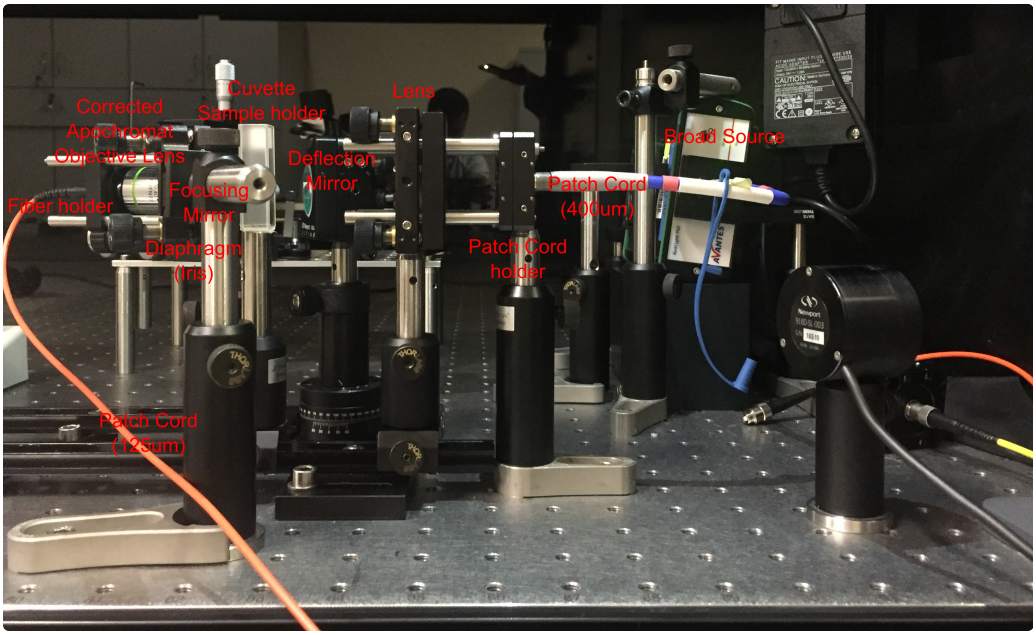

Figure 2. A simple spectrometer setup for absorption spectroscopy.

source as shown in Fig. 2 is the tungsten halogen lamp from Avantes (Avalight HAL). The light source supports wavelengths in the range from 380 nm to 2500 nm. A collimating lens was attached to the casing of the source to provide effective light coupling into the fiber patch cord. The core size of the fiber patch cord is 400 μm providing a better medium for the broad source to transmit through the fiber patch cord. The biconvex lens in the setup was to focus the light into a cuvette and also into the aperture of a detector. This bi-convex lens is coated for the wavelength range of 600 nm until 1200 nm. Such a lens was to make sure that all the light rays pass through the cuvette. Thus, the spot size of the light reaching the cuvette would be less than the width of the cuvette. This was to allow optimum absorption on each of the transmitted wavelengths.

The first mirror deflects the light into the second mirror. These mirrors help to adjust the light to be transmitted into the center point of the iris aperture before reaching the photodetector. The second mirror provided an additional adjustment of the light. Therefore, the second mirror had a wider control of light deflection into the detector while the first mirror had limited control of deflection. The rotation stage on the second mirror gives the flexibility of

the X-Y adjustment of the mirror. These two mirrors systems were intended for a compact optical setup. Thus, a two-mirror configuration gives flexibility in reducing the size of the optical setup and allows easy adjustment on the light path of optical alignment.

In this experiment, the light is a source of vibration energy that will interact with the sample that place in the cuvette. After the optical setup was ready, the optimization of the signal was done to get optimize light signal enter into the detectors. Before the absorption spectra were measured, the background noise of the system was detected and becomes the reference background power. In this background test, all cuvette that will be used was measured its background source to check the background power. Then, the sample was placed in the cuvette for measurement of the absorption value. The light that enters the iris was directly focused by an objective lens into a multimode fiber which a core size of 125 μm. The light emitted from the fiber was directed into a cuvette that contains a sample before reach a grating. The light then being diffracted into the detector. The diffraction grating splits the light into many wavelengths which were then captured by an array of detectors. In this experimental setup, an optical spectrum analyzer (OSA) was used to diffract and collect the light measurement. The optimization of light coupling in the objective lens was done using a Si-free space detector. The detector gives the Root mean square (RMS) value of the light signal and optimization was done based on the best RMS value rather than the spectrum of the signal. The results taken were results that were collected repeatedly to check the consistency with the absorption spectra.

The setup gives the flexibility to reduce the size of the spectrometer as mention before. In our setup, the focusing of the light into the sample becomes more simple since the deflection signal made the broad spectra can be easy to focus on the cuvette. As in a normal spectrometer, the broad source needs to be aligned and focus on the sample and the arrangement of mirrors in a straight line that focuses on the sample makes the system is bulky and sensitive to the vibration effects. Even this configuration using the current method reduces into micro-miniature optics, the setup still has a bigger size compared to our design.

3. Results and discussion

The position of lenses and the distance between the lenses and receiver was studied. This is to improve the intensity of the intended wavelength to pass through the optical setup with minimal losses. Thus, we can improve the power margin for our absorption spectra signal at the detector later. The result shows that the distance of the lenses does affect the coupling efficiency as shown in Fig. 3. The position of 70 mm away gives optimum coupling efficiency. The graph also shows that the pattern of coupling efficiency swings between convergence and divergence as the distance is varied. This result also agrees with our references, [18], [19], in such when the optic ray converges the amount of light into the detector is more compared to when it diverges. In our study, we found that, even though the convergence and divergence happen, the absorption value cannot be measured until it reaches the optimum point of 70 mm. In the region away from the optimum point, our absorption shows noises where the detector was not able to distinguish between the absorption value and environmental noise. At the optimum point, the absorption of spectra can be detected even though the light coming from the source is attenuated down. It has shown that no absorption points were able to be detected when the coupling efficiency was not at the optimum point with the light attenuated. Experimentally, we also study the effect of the worst-case scenario of our setup where the light was attenuated by using different wavelength coatings in the mirrors as shown in Fig. 4.

In Fig. 4, the result shows the absorption values at high attenuation conditions when the light entering the detector is minimal. As mentioned previously in Section 2.1, there is a location of the optimum position. We conduct the experimental test and locate the lenses position based on the result shown in Fig. 3. Initially, we placed our lenses at the optimum point and we measured the input signal and also the output signal. Then we moved into other positions with the same setup. We found that only at the optimum point we can measured the signal absorption. The same amount of receiving power that produced the signal when the lenses were in the optimum position cannot produced any signal and only produced noises value when not in that optimum position. However, at the optimum point, we can classified the absorption situation as the point where high absorption occurs and where there was a minimal occurrence of absorption. As presented in Fig. 4; it is shown that where the occurrence of absorption is minimal, the amount of peaks is less compared to where the occurrence of absorption is maximum where more peaks are located there. The maximum absorption and minimum absorption locations are labeled as main absorption and minimum absorption respectively. Based on this result, we found that whenever we found this peak, the system is already in the optimum position. Then the only parameter that can be adjusted to have good visibility of the optical signal received by improving the intensity of the signal since the optical setup is already in optimum condition.

The light interaction with the sample can be as a reflection, refraction, absorption, scattering, diffraction, or transmission. Signal loss from the sample can occur as specular reflection, internal scattering, refraction, complete absorption, transmission loss during reflectance measurement, and trapping loss. During measurement, the light enters the sample and interacts resulting either in attenuated transmitted light or reflected light. The light frequency and the

https://doi.org/10.53655/joe.c1987k

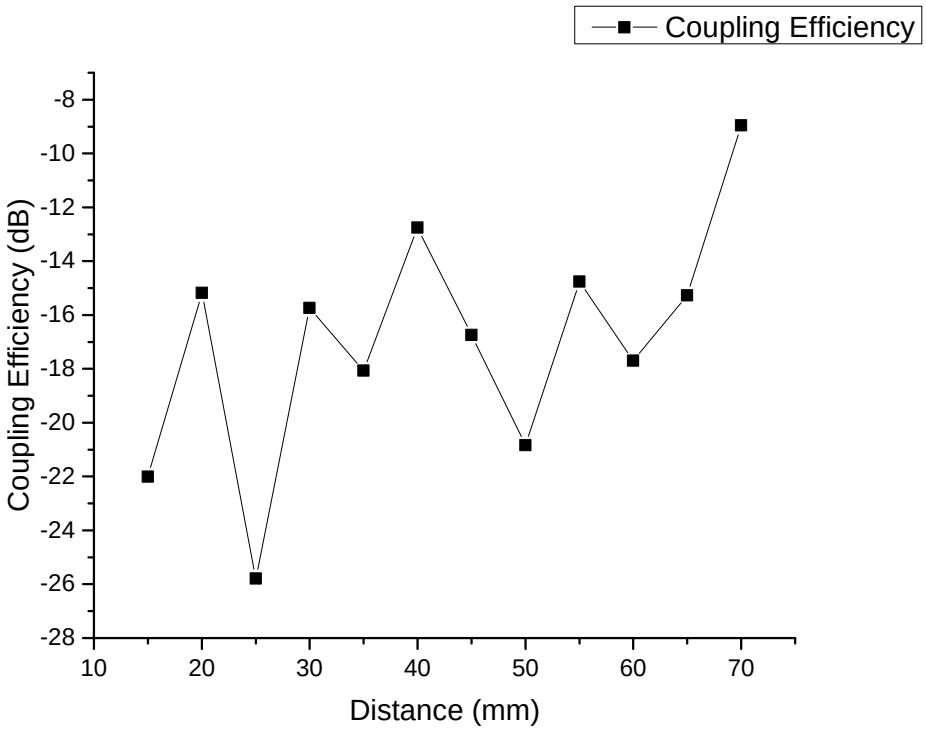

Figure 3. The coupling efficiency pattern based on the position of the detector from the lens using simulation.

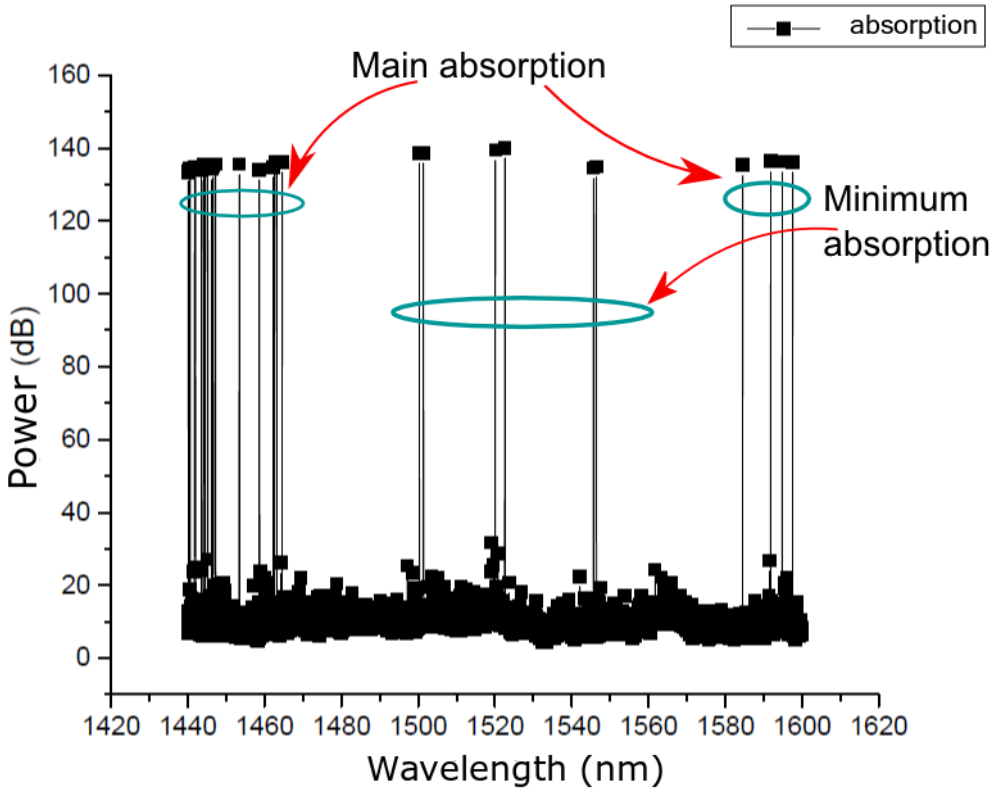

Figure 4. The absorption signatures in high attenuation region or low scattering light

amount of light being absorbed would yield information regarding both the physical and chemical compositional information of a sample.

In this experiment, we first observed the absorption peak for dichloromethane (DCM) in liquid form. The experiment was initially focused on the visible range since most of the studies are focusing on the same range[20].However, in this region, there is a tendency that DCM produces fluorescence emission [20]. In the beginning, our result only verifies the absorption wavelength peak but the noise floor is too high which forbids us from quantifying the result. This is also worsened by the other bonding overtones that happen in the visible region [21]. Thus, we expand our optical system into the short NIR region and focus on Deionized Water (DI) water first because the absorption of DI water [22] falls in this region. From our experimental result, the first absorption spectra of DI-water fall in the range of 900 nm until 1100 nm which tallies with other studies [23], [24]. DI water has been used as a reference model due to its availability and easiness of handling. Thus we focus on this range of wavelength for sample characterization as DI water absorption can be detected here. Besides, during our experimental investigation, we found DI water's isosbestic point falls under the wavelength of interest. This is an advantage for the optical setup which can use the isosbestic point as the reference point and calibration point.

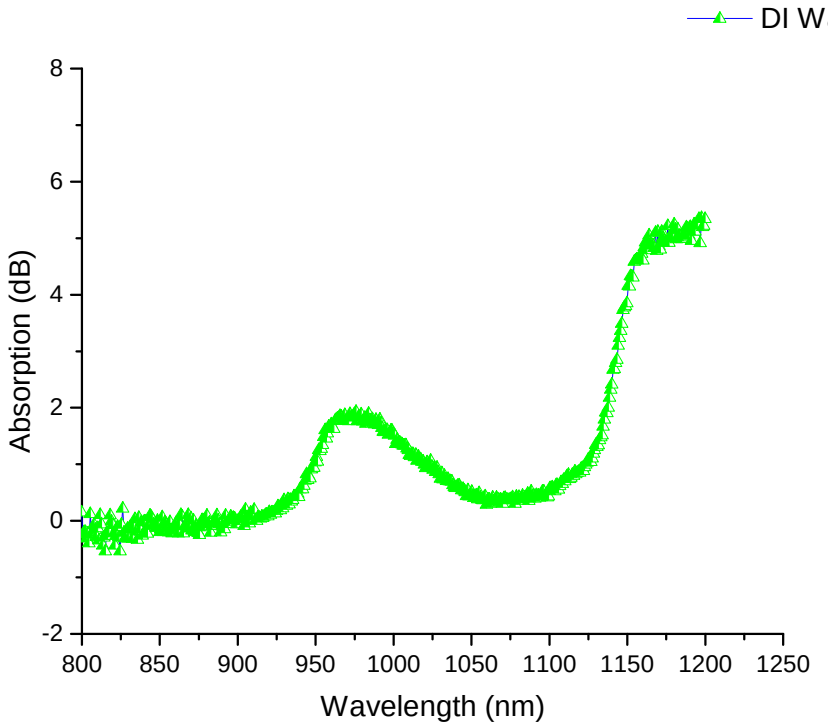

Figure 5. The absorption spectra for DI water.

The DI water absorption peak is found at the wavelength of 970 nm and this result tallies with other experimental results [25], [26]. This peak is referred to as the isosbestic point and is commonly used for calibration because the total absorbance of a sample does not change with a chemical reaction or physical change of the sample such as its temperature [27] or pH. Other absorption peaks of water normally change with ambient temperature, wherein in our case the room temperature was around 25°C, thus producing a broad absorption peak at 1100 nm wavelength. The point can be identified by changing the chemical content of DI water or increasing the temperature. The new curves cross the same point (isosbestic point) even though the chemical content of DI water has changed. DI water absorption result is important for us to classify our C-H bond since most of the solution or solvent contains hydrogen bond which normally overlapping to C-H bond [28]. Thus, the result confirms that our hydrogen bond or O-H bond does not affect our result and the spectrum of the C-H bond does not have any overlapping spectrum from the O-H bond.

As shown in Fig. 6 the graph is the absorption result of wavelength spectra using several samples in liquid form. This result shows a second harmonic and the third harmonic of vibration due to the C-H bonding [27]. DCM is categorized under methylene group, CH_2, and our result shows that the second overtone falls at the wavelength of 1149 nm which agrees with the result Workman Jr & Weyer [27]. It can also be observed the third overtone is

https://doi.org/10.53655/joe.c1987k

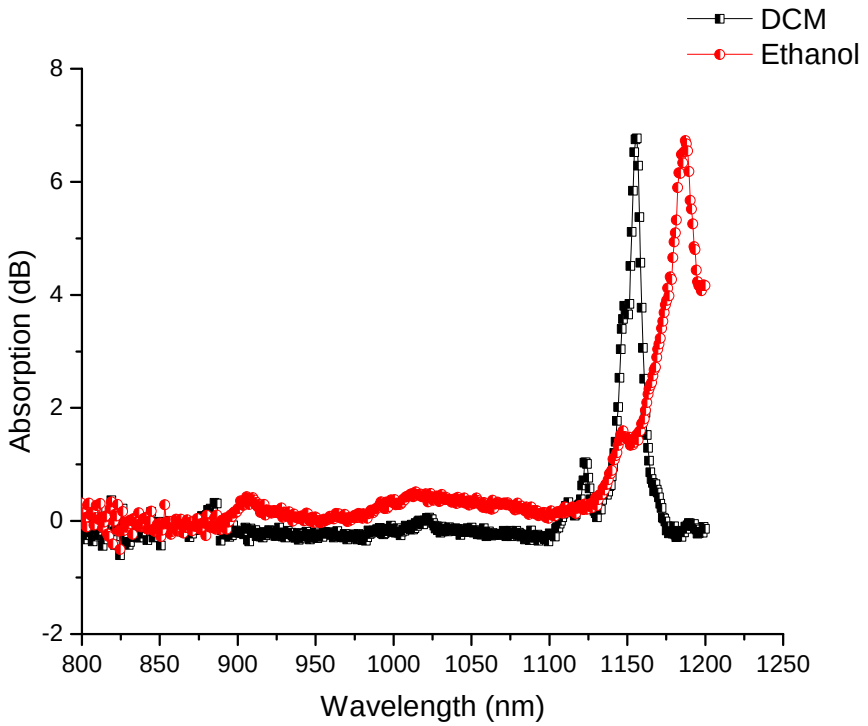

Figure 6. The absorption spectra for the DCM and ethanol produce by simple optical setup.

at 870 nm, however, this peak is low in intensity. Fig. 6 also shows the C-H bond which includes ethanol. The second overtone has combination tones, which can also be seen at the ethanol spectrum where the peak broadens and is shifted into 1200 nm. The peak at the wavelength between 1100 nm till 1300 nm gives the signature of the C-H bond. Based on these two samples, it can be seen that the C-H bond has two peaks which give indications of the C-H bond inside the sample. This can be utilized in our application to detect the C-H bond to identify tissue malignancies for early cancer detection. As mentioned previously in the Introduction section, the C-H bond can be used as a parameter to detect tissue malignancies.

In order to confirm our experimental technique, we also tested two unknown samples with our experimental setup to identified the ability of our setup to detect the C-H bond. The results are shown in Fig. 7 where we label it as Solvent 1 and Solvent 2. These solvents were randomly picked from our laboratory without any label of the sample. These solvents were tested and two solvents showed the same spectra absorption as similar to DCM and ethanol. These two solvents were prepared to have the C-H bond in their chemical bonds. Both solvents were unknown to the authors initially and then we matched these two solvents in our laboratory repository to identified these two solvents based on chemical bond and reaction. They are Dimethyl sulfoxide and Diethyl ether. The spectra on which these two solvents behave were unknown. Based on the previous result as shown in Fig. 6, we can identify that Solvent 1 corresponds to Dimethyl sulfoxide and Solvent 2 is Diethyl ether. The result shows the effect of the Carbon component in the C-H bonding which shifts the spectrum toward 1200 nm. It can be further identified based on the small peak at each of the high peaks. The result shows that the small peak broadens and almost combine if there are more than one Carbon component and more Hydrogen components. This shows the availability of the C-H bond to be identified, classified, and quantified. This can be more accurate with the Chemometrics procedure in analyzing these peaks. The absorption peak also able to identify C-H bonding on the various chemical group as shown in the above results. This validates the new result that shows that the C-H bond can be classified by region bond under NIR wavelength. It is thus proved that this setup can detect the C-H bond to identify tissue malignancies.

4. Conclusion

The optical setup for spectroscopy yields efficient results for measuring the absorption spectra and can reduce the need for having high complexity and a complete spectrometer system for chemical analysis. This simple system can identify the C-H bond to classify tissue malignancies. The simulation process makes the experimental result more

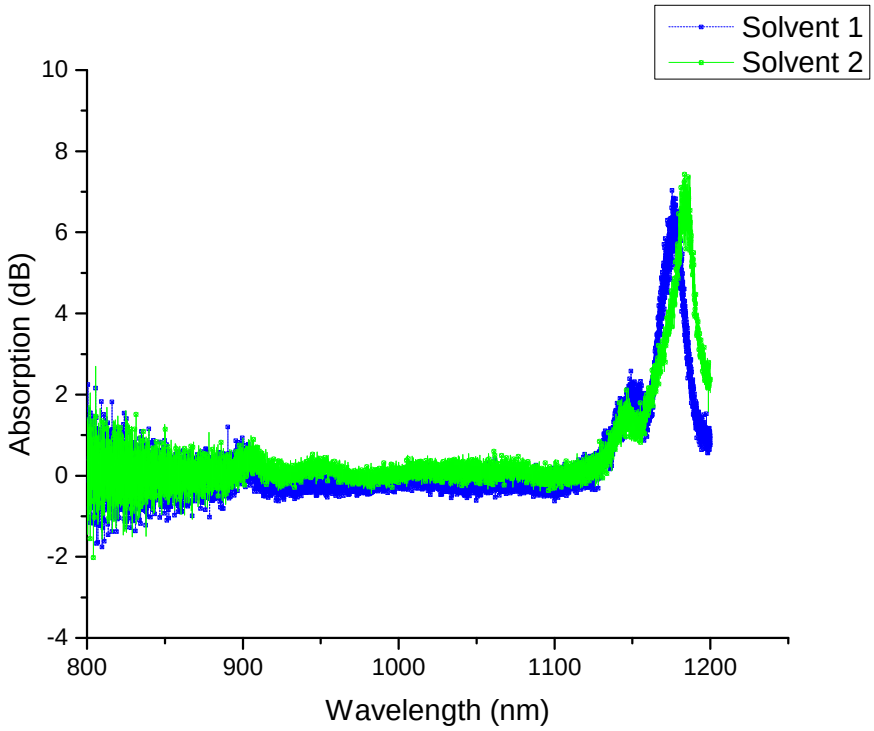

Figure 7. The absorption signatures for two unknown solvents which have content C-H bond.

precise especially constructing the optical setup. The experimental results show a wavelength range from 600 nm to 1200 nm can measure and analyze the C-H chemical bonding to give an absorption spectra at a range of 1100 nm to 1200 nm. The result also shows the ability to quantify the chemical bond of a sample based on two peaks of absorption due to the C-H bonding. This gives a better opportunity for Chemometrics to perform accurately. In this setup as well, the stable calibration point is identified which corresponds to the isosbestic point of DI water at 970 nm. This is the point where the result may be rectified if the spectra are shifted due to misalignment or the quality of the source. This proved that this simple optical setup is not only able to produce better C-H bond results but also consistent results.

Acknowledgments

The authors would like to thank Ms. Noor Nazurah for her assistance in the chemical explanation and share collection of references. Thanks to Mr. Zaliman in assisting and providing some free-space optic components. NA also thank Ms. Norazah Abdul Rashid for providing the unknown samples which contain C-H bond. The author would like to acknowledge the support from the Fundamental Research Grant Scheme (FRGS) under a grant number of FRGS/1/2020/STG07/UNIMAP/02/3 from the Ministry of Education Malaysia. The authors also would like to acknowledges support from Opto-Biochemical Lab for providing the space for this experimental setup and equipment from RMK9 Malaysia grant. Some of the tools are utilized from TechnoFund (Grant No: TF0313D187)

References

[1] J. Ribaudo, "Balloon and button spectroscopy: A hands-on approach to light and matter," *The Physics Teacher*, vol. 54, no. 6, pp. 330–334, 2016. DOI: 10.1119/1.4961171.

[2] L. H. Lajunen and P. Peramaki, *Spectrochemical Analysis by Atomic Absorption and Emission*. The Royal Society of Chemistry, 2004, pp. X001–X004, ISBN: 978-0-85404-624-9. DOI: 10.1039/9781847551900.

[3] J. M. Hollas, *Modern spectroscopy*. John Wiley & Sons, 2004, ISBN: 978-0-470-84416-8.

[4] A. Arons and M. Peppard, "Einstein's proposal of the photon concept—a translation of the Annalen der Physik paper of 1905," *American Journal of Physics*, vol. 33, no. 5, pp. 367–374, 1965.

https://doi.org/10.53655/joe.c1987k

[5] G. Reich, "Near-infrared spectroscopy and imaging: Basic principles and pharmaceutical applications," *Advanced drug delivery reviews*, vol. 57, no. 8, pp. 1109–1143, 2005. DOI: 10.1016/j.addr.2005.01.020.

[6] Y. Roggo, P. Chalus, L. Maurer, C. Lema-Martinez, A. Edmond, and N. Jent, "A review of near infrared spectroscopy and chemometrics in pharmaceutical technologies," *Journal of pharmaceutical and biomedical analysis*, vol. 44, no. 3, pp. 683–700, 2007. DOI: 10.1016/j.jpba.2007.03.023.

[7] B. Waruru, K. Shepherd, G. Ndegwa, A. Sila, and P. Kamoni, "Application of mid-infrared spectroscopy for rapid characterization of key soil properties for engineering land use," *Soils and Foundations*, vol. 55, no. 5, pp. 1181–1195, 2015. DOI: 10.1016/j.sandf.2015.09.018Get.

[8] K. Kong, C. Kendall, N. Stone, and I. Notingher, "Raman spectroscopy for medical diagnostics—from in-vitro biofluid assays to in-vivo cancer detection," *Advanced drug delivery reviews*, vol. 89, pp. 121–134, 2015. DOI: 10.1016/j.addr.2015.03.009.

[9] C. Wang, Z. Wang, T. Zhao, *et al.*, "Optical molecular imaging for tumor detection and image-guided surgery," *Biomaterials*, vol. 157, pp. 62–75, 2018. DOI: 10.1016/j.biomaterials.2017.12.002.

[10] S. Koljenovic, T. B. Schut, R. d. Wolthuis, *et al.*, "Tissue characterization using high wave number Raman spectroscopy," *Journal of biomedical optics*, vol. 10, no. 3, pp. 031 116–03 111 611, 2005. DOI: 10.1117/1.1922307.

[11] D. A. Burns and E. W. Ciurczak, *Handbook of near-infrared analysis*. CRC press, 2007, ISBN: 9780849373930.

[12] A. Alfonso-Garcia, R. Mittal, E. S. Lee, and E. O. Potma, "Biological imaging with coherent Raman scattering microscopy: A tutorial," *Journal of biomedical optics*, vol. 19, no. 7, pp. 071 407–071 407, 2014. DOI: 10.1117/1.jbo.19.7.071407.

[13] M. T. Cicerone, K. A. Aamer, Y. J. Lee, and E. Vartiainen, "Maximum entropy and time-domain Kramers–Kronig phase retrieval approaches are functionally equivalent for CARS microspectroscopy," *Journal of Raman Spectroscopy*, vol. 43, no. 5, pp. 637–643, 2012, ISSN: 1097-4555. DOI: 10.1002/jrs.3169.

[14] R. Oeschger, B. Su, I. Yu, *et al.*, "Diverse functionalization of strong alkyl C–H bonds by undirected borylation," *Science*, vol. 368, no. 6492, pp. 736–741, 2020. DOI: 10.1126/science.aba6146.

[15] G. A. Jardim, D. J. Lima, W. O. Valença, *et al.*, "Synthesis of selenium-quinone hybrid compounds with potential antitumor activity via Rh-catalyzed CH bond activation and click reactions," *Molecules*, vol. 23, no. 1, p. 83, 2018. DOI: 10.3390/molecules23010083.

[16] F. J. Duarte, "Ray transfer matrix analysis of multiple-prism dye laser oscillators," *Optical and Quantum Electronics*, vol. 21, no. 1, pp. 47–54, 1989. DOI: 10.1007/BF02199466.

[17] F. J. Duarte, "Dispersive dye lasers," in *High-Power Dye Lasers*, F. J. Duarte, Ed., Springer, 1991, pp. 7–43. DOI: 10.1007/978-3-540-47385-5_2.

[18] D. Malacara-Hernández and Z. Malacara-Hernández, *Handbook of optical design*. CRC Press, 2013, ISBN: 9781439867990.

[19] A. Schuster, *An introduction to the theory of optics*. E. Arnold, 1904.

[20] S. H. Nabavi, M. H. Khodabandeh, M. Golbabaee, A. Moshaii, and M. D. Davari, "Excited states study reveals the twisted geometry induced large stokes shift in DCM fluorescent dye," *Journal of Photochemistry and Photobiology A: Chemistry*, vol. 354, pp. 127–138, 2018. DOI: 10.1016/j.jphotochem.2017.05.017.

[21] H. Maeda, N. Eifuku, Y. Haketa, Y. Ito, E. Lee, and M. Lee, "Water-supported organized structures based on wedge-shaped amphiphilic derivatives of dipyrrolyldiketone boron complexes," *Physical Chemistry Chemical Physics*, vol. 13, no. 9, pp. 3843–3850, 2011. DOI: 10.1039/C0CP02294B.

[22] B. Hou, D. Zhang, S. Zhao, *et al.*, "Scalable and dii-compatible optical clearance of the mammalian brain," *Frontiers in neuroanatomy*, vol. 9, 2015. DOI: 10.3389/fnana.2015.00019.

[23] G. M. Hale and M. R. Querry, "Optical constants of water in the 200-nm to 200-μm wavelength region," *Applied optics*, vol. 12, no. 3, pp. 555–563, 1973. DOI: 10.1364/AO.12.000555.

[24] J. Jeon, S. Park, and B. J. Lee, "Optical property of blended plasmonic nanofluid based on gold nanorods," *Optics express*, vol. 22, no. 104, A1101–A1111, 2014. DOI: 10.1364/OE.22.0A1101.

[25] H. Yamatera, B. Fitzpatrick, and G. Gordon, "Near infrared spectra of water and aqueous solutions," *Journal of Molecular Spectroscopy*, vol. 14, no. 1, pp. 268–278, 1964. DOI: 10.1016/0022-2852(64)90121-3.

[26] K. Buijs and G. Choppin, "Near-infrared studies of the structure of water. i. pure water," *The Journal of Chemical Physics*, vol. 39, no. 8, pp. 2035–2041, 1963. DOI: 10.1063/1.1734579.

[27] J. Workman Jr and L. Weyer, *Practical guide and spectral atlas for interpretive near-infrared spectroscopy*. CRC Press, 2012, ISBN: 9781439875254.

[28] Z. Wu, G. Ouyang, X. Shi, Q. Ma, G. Wan, and Y. Qiao, "Absorption and quantitative characteristics of CH bond and OH bond of NIR," *Optics and Spectroscopy*, vol. 117, no. 5, pp. 703–709, 2014. DOI: 10.1134/S0030400X1411023X.

https://doi.org/10.53655/joe.c1987k